Role of Frequency Chirp and Energy Flow Directionality in the Strong Coupling Regime of Brillouin-Based Plasma Amplification

M. Chiaramello,[1] F. Amiranoff,[1] C. Riconda,[1] and S. Weber[2]
[1]LULI—UPMC Université Paris 06: Sorbonne Universités, CNRS, École Polytechnique, CEA: Université Paris-Saclay, F-75252 Paris cedex 05, France
[2]Institute of Physics of the ASCR, ELI-Beamlines, 18221 Prague, Czech Republic
(Received 12 September 2016; published 2 December 2016)

A detailed analysis is presented of the various stages of strong coupling Brillouin plasma amplification, emphasizing the importance of the chirp which can be of threefold origin: the intrinsic one driven by the amplification process, the one originating from the chirped-pulse-generated laser pulses, and the one associated with the plasma profile. Control of the overall chirp can optimize or quench the energy transfer. The time-dependent phase relation explains the energy flow direction during amplification and is characteristic for this strong coupling process. The study is also of potential importance to understand and maybe control cross-beam-energy transfer in inertial confinement fusion.

DOI: 10.1103/PhysRevLett.117.235003

Plasma optics is a promising and powerful way to manipulate coherent light at intensities which cannot be handled by solid-state optical materials [1,2]. Plasma photonic devices also allow for the dynamic control of laser beams in general [3–5]. Exploiting three-wave coupling processes in plasmas has received considerable attention over the past few years as a new way to create short and intense pulses over large cross sections [6–31], which are subsequently focused using plasma devices [32–34]. This opens up the way for future exawatt laser systems [35,36] such as the proposed fourth pillar of the Extreme Light Infrastructure (ELI) [37] or Exawatt Center for Extreme Light Studies [38]. In order to attain short time scales, the suitable three-wave coupling processes [39,40] are based on either Raman backscattering (SRS) [6–8,10–14,16,26,31] or strong coupling Brillouin backscattering (SCSBS) [9,15,17–25,27–30]. In this Letter, SCSBS is considered and the process is discussed in detail from the initial coupling up to the self-similar regime [9]. In particular, it is shown that, in contrast to the weak coupling regime of Brillouin backscattering, Raman backscattering, and standard optical parametric amplification (OPA) techniques [41], the phase relation of the constituent waves, transverse electromagnetic and longitudinal compressional, is continuously time dependent. The time dependence of the total phase of the three implicated waves explains the energy flow direction during the amplification process and determines the quality of the amplification. This temporal dependence results in a time-dependent frequency of either a seed, electrostatic wave, or pump (analogous of a chirp). Once the evolution of the intrinsic chirp for given interaction conditions is understood, the contributions from the laser pulse and the plasma profile allow us to partially control the overall chirp and optimize or quench the amplification process. This understanding allows us to improve the experimental interaction process [42,43]. Previous spatiotemporal analysis of SCSBS for long (nanosecond) pulses were limited to the regime where pump depletion is negligible [44] or to a regime dominated by flow inhomogeneities [45]. More recently, in the context of plasma amplification and relatively short pulses, it was pointed out by numerical analysis that the sign of the laser chirp is important in SCSBS coupling for a homogeneous plasma [24], in contrast to the symmetric effect of laser chirp in the weak coupling SBS regime [23] or the SRS regime [8]. However, no scaling laws were derived, and the approach was not based on the analysis of the waves' phases.

The strong coupling regime of Brillouin backscattering is characterized by the fact that the density perturbation envelope varies quickly over an acoustic period. Therefore, the second derivative in the plasma response needs to be retained:

$$
\begin{aligned}
(\partial_t + v_g^p \partial_x) E_p &= -i \frac{\omega_{pe}^2}{4\omega_0} N E_s e^{-i(\omega_{0s}-\omega_0)t}, \\
(\partial_t - v_g^s \partial_x) E_s &= -i \frac{\omega_{pe}^2}{4\omega_{0s}} N^* E_p e^{-i(\omega_0-\omega_{0s})t}, \\
(\partial_t^2 - c_s^2 \partial_x^2) N &= -\frac{2Ze^2}{m_e m_i c^2} E_p E_s^* e^{-i(\omega_0-\omega_{0s})t}. \qquad (1)
\end{aligned}
$$

E and $N = \delta n/n_e$ are the electromagnetic field and density perturbation, respectively. The indices p and s refer to the pump pulse and the seed pulse, respectively, and ω_0 and k_{0p} are the pump frequency and wave vector, respectively. The density perturbation wave vector is k, with $k \simeq 2k_{0p}$, and $v_g = c\sqrt{1 - n_e/n_c}$ is the group velocity of the corresponding electromagnetic waves, $c_s = \sqrt{ZT_e/m_i}$ the ion sound

velocity, and $\omega_{pe} = \sqrt{n_e e^2/m_e \epsilon_0}$ the background electron plasma frequency. These equations describe the energy coupling between the three waves up to and including pump depletion. In this SCSBS regime, the unstable ion-acoustic wave is a driven quasimode characterized by $\omega = \omega_{SC} + i\gamma_{SC} = (k_{0p}^2 v_{osc}^2 \omega_{pi}^2/2\omega_{0p})^{1/3}[\frac{1}{2} + i(\sqrt{3}/2)]$. Here γ_{SC} [46] is the growth rate for SCSBS, which generates very short time scales approaching the ones of SRS. This allows us to use short pump and seed pulses in the regime of picoseconds and hundreds of femtoseconds. As such pulses are generated by chirped pulse amplification [47,48], the chirp needs to be accounted for in the analysis. In the following, a chirp α is included in the pump laser field (as only the total chirp, of a pump and/or seed, matters), $E_p \propto e^{i[k_{0p}x - \omega_0 t + \phi(x,t)]}$, where to linear order the phase variation is $\phi(x,t) = \alpha[k_{0p}(x - x_0) - \omega_0(t - t_0)]^2$, generating a time-dependent frequency as $\omega(x,t) = \omega_0 - [\partial\phi(x,t)/\partial t]$. The complete set of equations describing the evolution of the three amplitudes and phases takes the form, for $\omega_0 = \omega_{s0}$ and in the limit $c_s \ll v_g^{p,s}$,

$$
\begin{aligned}
(\partial_t \pm v_g^{p,s}\partial_x)E_{p,s} &= \mp \mu N E_{s,p} \sin\vartheta, \\
(\partial_t + v_g^p \partial_x)\varphi_p &= -\mu \frac{N E_s}{E_p}\cos\vartheta, \\
(\partial_t - v_g^s \partial_x)\varphi_s &= -\mu \frac{N E_p}{E_s}\cos\vartheta, \\
\partial_t^2 N - N(\partial_t \varphi)^2 &= -\Lambda E_p E_s \cos\vartheta, \\
N\partial_t^2\varphi + 2\partial_t N \partial_t \varphi &= -\Lambda E_p E_s \sin\vartheta,
\end{aligned}
\tag{2}
$$

with $\mu = (\omega_{pe}^2/4\omega_0)$ and $\Lambda = (2Ze^2/m_e m_i c^2)$ the coupling factors for the field and density perturbations, respectively. With these definitions, one has $\gamma_{SC} = [(3\sqrt{3}/8)\mu\Lambda E_p^2]^{1/3}$. In Eqs. (2), $\vartheta = \varphi_p - \varphi_s + \phi - \varphi$ is the global phase. In contrast to the weak coupling SBS and SRS regimes, or OPA, the optimal phase for coupling in these equations is not evident *a priori*, since it appears in a nonsymmetric way in the transverse wave equations and ion-acoustic wave equation. However, estimates can be derived for the phases dynamics at three different stages of the interaction: in the initial seed growth (SI), in the "linear" growth phase, when pump depletion is negligible and seed and density perturbation grow exponentially (SII), and when the growth saturates and the energy flow is reversed (SIII). In the following, the above set of equations is fully solved numerically using explicit finite differencing and the physics discussed. The equations cover the temporal evolution of the three main stages of the amplification process. Figure 1 shows the time evolution for a typical case with parameters $I_p = 10^{15}$ W/cm^2, $I_s = 10^{13}$ W/cm^2, and $\lambda = 1$ μm. Both pulses are semi-infinite and cross in the middle of a constant density plasma of 600 μm in length and $n = 0.1$ n_c. Here the chirp α is set to zero. These values

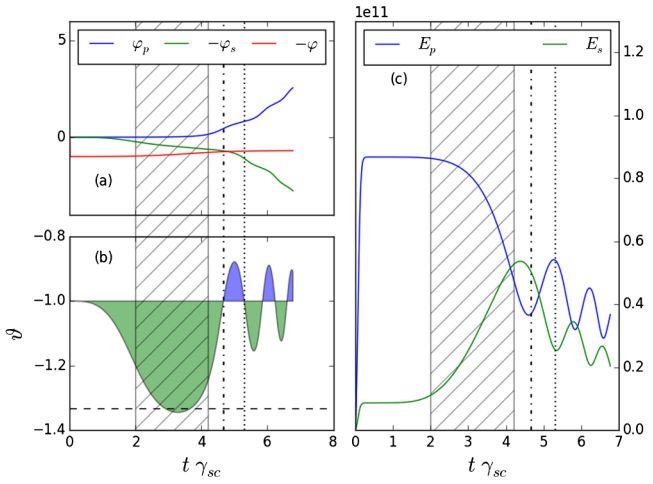

FIG. 1. (a) Evolution in time of the phases of the pump (φ_p, blue line) and of the seed ($-\varphi_s$, green line) and the density perturbation ($-\varphi$, red line) in units of π. (b) Time evolution of the total phase $\vartheta = \varphi_p - \varphi_s + \phi - \varphi$, in units of π. The green shadowed regions indicate the values of ϑ for which the pump amplifies the seed; the blue ones correspond to a reversed flow energy direction. (c) Electric field amplitudes, in V/m, of the pump (blue line) and of the seed (green line) as a function of time. The data are taken at $x_{cross} = 350$ μm, the point where seed and pump initially collide in the plasma.

correspond to $\gamma_{SC} \approx 4.29 \times 10^{12}$ Hz, or $\tau_{SC} \equiv 1/\gamma_{SC} = 233$ fs.

SI: Initial growth.—The subsequent analysis uses $\varphi_p = \varphi_s = 0$ at $t = 0$ with no loss of generality. As initially $\partial_x = 0$ and $N = 0$, one obtains at the crossing point $N \sim -\Lambda E_p E_s(\cos\vartheta)(t^2/2)$. Since N is defined as a positive quantity, this implies $\vartheta = -\pi = -\varphi$ [49]. As a consequence, the equations for the phases of a pump and seed [see Eqs. (2)] become $\partial_t \varphi_p = \mu N E_s/E_p$ and $\partial_t \varphi_s = \mu N E_p/E_s$. Initially, the field amplitudes are taken as positive. As $E_p \gg E_s$ by construction, one obtains $\partial_t \varphi_s \gg \partial_t \varphi_p \approx 0$; i.e., φ_p will remain zero and $\vartheta \approx -\pi + \varphi_p - \varphi_s < -\pi$ [see the phase evolution in Fig. 1(a)]. Still within the limit of the approximation above, one can derive from these equations $\varphi_s(t) = \frac{2}{9\sqrt{3}}\gamma_{SC}^3 t^3$. It follows from the amplitude equations that $\partial_t E_s > 0$ and $\partial_t E_p < 0$ and the energy flows from the pump to the seed [green shaded region in Fig. 1(b)]. During this stage (SI), the total phase has the time dependence $\vartheta(x = x_{cross}, t) = -\pi - (2/9\sqrt{3})\gamma_{SC}^3 t^3$. This phase relation is valid in the time interval $0 < t\gamma_{SC} < 2$, as can be seen in Fig. 1(b) and as calculated in the following section.

SII: Exponential growth.—During this linear stage, pump depletion is still negligible and the seed intensity grows exponentially. This means that the seed phase evolves as $\varphi_s = (\gamma_{SC}/\sqrt{3})t + \varphi_{s0}$ and the density phase in the opposite way, such that the total phase remains approximately constant. This is confirmed by the numerical

solution. By setting exponential growth for the density and seed amplitude in Eqs. (2), one can derive that in this regime the total phase is given by $\vartheta = -\frac{4}{3}\pi$. The time required to attain this regime is given by setting $\varphi_s(t)$ (from SI) equal to $(\pi/3)$:

$$t_i = \left(\frac{3\sqrt{3}\pi}{2\gamma_{\mathrm{SC}}^3}\right)^{1/3} \approx \frac{2}{\gamma_{\mathrm{SC}}}, \tag{3}$$

consistent with the numerical results [Fig. 1(b)]. The system will stay in this regime as long as pump depletion is negligible. The time t_{exp} during which the exponential regime holds until pump depletion starts and the solution enters the self-similar regime can be evaluated making the hypothesis that $E_s \approx E_p$ at the end of the exponential regime, with E_{s0} indicating the initial value of the seed amplitude. This results in a time that is comparable to the initial growth time:

$$t_{\mathrm{exp}} = \frac{1}{\gamma_{\mathrm{SC}}} \ln \frac{E_{p0}}{E_{s0}} = \frac{1}{2}\frac{1}{\gamma_{\mathrm{SC}}} \ln \frac{I_{p0}}{I_{s0}}. \tag{4}$$

The total time necessary to reach pump depletion is then given as $t_{\mathrm{depl}} = t_i + t_{\mathrm{exp}} = (1/\gamma_{\mathrm{SC}})[2 + 1.15 \log_{10}(I_{p0}/I_{s0})] \approx (4.3/\gamma_{\mathrm{SC}})$ for the given simulation parameters, corresponding to the shaded area in Fig. 1. *SIII: Saturation.*—Once pump depletion sets in, the phase of the pump starts to evolve according to the pump phase equation assuming on the right-hand side exponential growth for the seed and the density perturbation, with $N_0 \equiv N(x = 0, t = t_i)$:

$$\partial_t \varphi_p = \partial_t \left(\varphi_p - \frac{4\pi}{3}\right) = -\frac{N_0 E_{s0} e^{2\gamma_{\mathrm{SC}} t}}{E_{p0}} \cos\left(\varphi_p - \frac{4\pi}{3}\right). \tag{5}$$

Integrating the above equation, one obtains for the pump phase

$$\varphi_p \approx \frac{1}{2}\frac{I_{s0}}{I_{p0}} (e^{2\gamma_{\mathrm{SC}} t} - 1). \tag{6}$$

The characteristic time for the global phase ϑ to vary from $-4\pi/3$ to $-\pi$ (value at which the coupling is zero) is given by a variation of φ_p of $\pi/3$. Once $\vartheta = -\pi + \epsilon$, the energy flow from the pump to the seed is reversed, leading to the oscillations behind the principal peak. This is analogous of the typical π-pulse structure in the weak coupling regime. This time is of the order of

$$t_{\varphi_p} \approx \frac{1}{2\gamma_{\mathrm{SC}}} \log\left(\frac{2\pi}{3}\frac{I_{p0}}{I_{s0}}\right). \tag{7}$$

The time the electric field reaches its maximum is then given as $t_{E_{\mathrm{smax}}} \approx t_i + t_{\varphi_p} = 4.67/\gamma_{\mathrm{SC}}$. From this time onwards, the pump no longer provides energy to the seed.

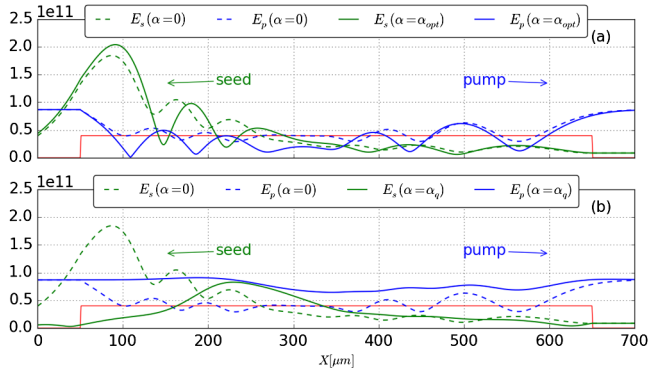

FIG. 2. Electric field amplitudes, in V/m, of the pump (blue lines, propagating to the right) and of the seed (green lines, propagating to the left) at $t = 1.5$ ps. Dashed lines are for $\alpha = 0$. Solid lines are for (a) $\alpha = \alpha_{\mathrm{opt}} \approx -3.3 \times 10^{-7}$ and (b) $\alpha = \alpha_q \approx 1.28 \times 10^{-6}$.

Role of the laser chirp.—A chirp induces a time variation of the total phase which will affect the coupling and therefore the efficiency of the energy transfer. Since the phase time dependence due to strong coupling is not the same as the one associated with the laser chirp, they cannot compensate each other at all times. However, the previous analysis highlights at which stage of the amplification process the phase could be modified by the laser chirp in order to improve coupling. The pump phase is negligible till pump depletion sets in. Pump depletion corresponds to large energy transfer which is affecting the downshift of the seed frequency. Optimal coupling would then be achieved if the chirp is such that the pump phase time derivative compensates the seed phase derivative at the moment pump depletion occurs. Assuming $t_0 = 0$ and $x_0 = x_{\mathrm{cross}}$, this leads to the condition $\varphi_s' = \gamma_{\mathrm{SC}}/\sqrt{3} = 2|\alpha|\omega_0^2 t$ at $t = t_{\mathrm{depl}}$, and the optimal chirp of the pump (equivalent to an upshift of the pump by ω_{SC}) is given by

$$\alpha_{\mathrm{opt}} \approx -\frac{1}{2\sqrt{3}}\frac{\gamma_{\mathrm{SC}}^2}{\omega_0^2}\frac{1}{2 + 1.15 \log_{10}\frac{I_p}{I_s}}. \tag{8}$$

The corresponding simulation results are shown in Fig. 2(a). By comparing the chirped case (solid lines) with the standard one (dashed lines), we observe that the effect of the chirp is not only to increase the maximum intensity by 35% but also to bring the pump locally to full depletion resulting in a first peak with a well-defined temporal width. If instead the pump laser is chirped with a positive α (downshifted) in such a way that the variation of the phase due to the laser chirp at the beginning of the interaction is of the same order as φ_s, the seed phase does not manage to evolve and adapt to allow the coupling but stays roughly constant and close to zero at all times. Thus, if one sets $\phi = \alpha\omega_0^2 t^2 \sim \phi_s \approx (\pi/3)$ at $t = t_i$, one obtains the chirp value which induces quenching:

$$\alpha_q \approx 0.26 \frac{\gamma_{\mathrm{SC}}^2}{\omega_0^2}. \tag{9}$$

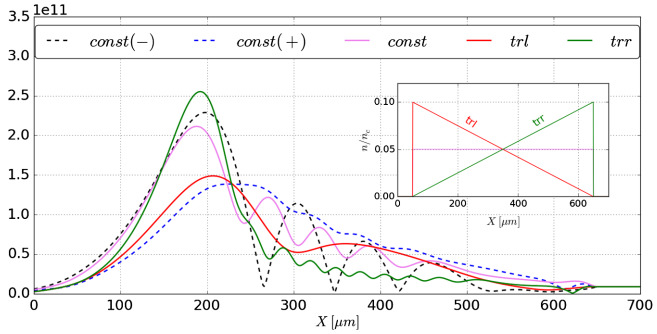

FIG. 3. Electric field amplitude of the seed as a function of space for const, constant density profile at $n_e/n_c = 0.05$ and no chirp; const(−), constant density profile with $\alpha = -2.7 \times 10^{-7}$; const(+), constant profile with $\alpha = +2.7 \times 10^{-7}$; and *trl* and *trr*, triangular density profiles with $n_{\max}/n_c = 0.1$.

Numerical solutions for this case are shown in Fig. 2(b). As we can see, the seed growth and energy transfer are very small. Notice that also a negative chirp much larger than α_{opt}, e.g., by an order of magnitude, will reduce the energy transfer. But in that case still some depletion occurs, and the result is much less dramatic than with a positive chirp.

Density profile effects.—Starting from Eqs. (2), neglecting the variations of v_g, and using the explicit density profile dependence of μ in the frame of reference of the seed pulse ($y = x - x_{\text{cross}} + v_g t$, $\tau = t$), one easily obtains the time evolution of φ_s:

$$\partial_\tau \varphi_s(y,\tau) = \mu(y)\frac{E_p}{E_s}N(y,\tau) = \frac{1}{2}\mu(y)\Lambda E_p^2\left(\frac{y}{v_g}\right)^2. \quad (10)$$

For a given profile, Eq. (10) can be integrated by assuming that the pump and seed initially cross at the right edge of the plasma (at $x_{\text{cross}} = 650$ μm in the numerical simulations; see the inset in Fig. 3) by keeping explicitly the spatial dependence. For, e.g., a linearly growing profile as seen by the pump ("trr" in Fig. 3), one has, with $x' = x - x_{\text{cross}}$,

$$\varphi_s(x',t) = \frac{4}{3\sqrt{3}}\gamma_{\text{SC,max}}^3\frac{|x'|}{v_g}\left(t - \frac{|x'|}{v_g}\right)^2\left(1 - \frac{1}{2}\frac{|x'|}{L}\right), \quad (11)$$

where $\gamma_{\text{SC,max}}$ is the value for the maximum density in the profile. The homogeneous case is found by taking the limit $L \to \infty$, and an analogous expression can be found for the decreasing profile as seen by the pump. A simple expression for the time when exponential growth sets in can be derived by considering the time t_i when the seed phase reaches the value $\pi/3$. This time is space dependent. In the inhomogeneous case, it is useful to find the position closest to the edge when the seed enters at first the exponential regime and the correspondent time by minimizing for t_i as a function of space. For a constant profile this gives $|x_i'| \approx 0.7(v_g/\gamma_{\text{SC}})$. For a linear ramp [with $v_g/(L\gamma_{\text{SC}}) \ll 1$] one obtains $|x_i'^{,trr}| \approx 0.7(v_g/\gamma_{\text{SC}})[1 - 0.12(v_g/L\gamma_{\text{SC,max}})]$ and $|x_i'^{,trl}| \approx 1.3(v_g/\gamma_{\text{SC,max}})(L\gamma_{\text{SC,max}}/v_g)$. It follows that the case trr is most favorable, as the seed enters earlier the exponential regime and the self-similar regime. In this respect, the homogeneous case is better if the density is equal to the maximum density, but it is less favorable if the density equals the average of the density ramp (see Fig. 3). Clearly visible, the case trr attains the highest amplification (an increase in maximum intensity of 40% with respect to the constant case and of a factor of ~3 with respect to trl). To have an order of magnitude estimate of the effect of a density gradient, one can define an effective pump chirp associated to the density gradient. The trr case is similar to the case of a negatively chirped pump, i.e., $\alpha < 0$, because the seed frequency downshift during the exponential regime is proportional to γ_{SC}, which decreases in magnitude. An effective chirp can thus be defined by posing in the middle of the profile ($x = -L/2$) $\omega(x) - \omega_0 = -2\alpha\omega_0 L/v_g \approx \gamma_{\text{SC,ave}}/\sqrt{3}$, with $\gamma_{\text{SC,ave}} = \gamma_{\text{SC}}(x = L/2)$. This leads to $\alpha = -(\gamma_{\text{SC,ave}} v_g/2\sqrt{3}\omega_0^2 L)$. An analogous calculation for the trl profile gives the same value of α but with the opposite sign. For the parameter used in the simulations $\alpha \approx \mp 2.7 \times 10^{-7}$. For the trr profile this value is close to the optimal chirp that can be calculated with Eq. (8) for the case const, $\alpha_{\text{opt}} \approx -2.1 \times 10^{-7}$. Simulations of amplification in an homogeneous profile with the effective chirps just calculated confirm the validity of this estimate, as the final amplified values become very close to the values found with the triangular profiles [compare the curve const(−) with the curve trr, and the curve const(+) with the curve trl in Fig. 3], even if there is more of a difference between the case with a density profile and the case with a chirp in the trailing pulses. In particular, for the case trr, the trailing peaks are very weak and the seed amplitude does not go to zero. A decreasing profile as seen by the seed leads to a larger amplification, favors the energy exchange mainly in the first peak, and at the same time allows us to control unwanted spontaneous instabilities (e.g., SRS) [27].

In conclusion, it was shown that a detailed analysis of the combined temporal evolution of amplitude and phase in the strong coupling regime allows us to clarify several issues in plasma amplification: the directionality of the energy flow and the role of the chirp originating from the laser pulse and the plasma profile. A definite relation was established between the maximum growth rate γ_{SC} and the condition for the laser chirp to allow optimal amplification or to quench the process. Contrary to SRS-based amplification, SCSBS requires a preferential gradient of the plasma profile with respect to the pump propagation direction. Even though this Letter focused on plasma amplification, the analysis presented is of relevance in a much wider sense. On the one side, it describes in detail for the first time a fundamental regime of three-wave coupling in plasmas by emphasizing the role of phases of the involved waves. On the other side, the analysis is of importance for specific application in the field of inertial confinement fusion (ICF)such as cross-energy-beam transfer [4,50] and speckles originating from random phase

plate as the interaction conditions can be in strong coupling. The chirp of long pulses (nanosecond) is negligible; however, the contributions from the plasma profile and the intrinsic interaction conditions remain for ICF.

M. C. and C. R. acknowledge support from Grant No. ANR-11-IDEX-0004-02, Labex Plas@Par. S. W. acknowledges support from the project ELI: Extreme Light Infrastructure (CZ.02.1.01/0.0/0.0/15-008/0000162) from European Regional Development. The authors acknowledge G. Lehmann for helpful discussions.

[1] B. C. Stuart, M. D. Feit, A. M. Rubenchik, B. W. Shore, and M.D Perry, Phys. Rev. Lett. **74**, 2248 (1995).
[2] *Laser-Induced Damage in Optical Materials*, edited by D. Ristau (Taylor & Francis, London, 2014).
[3] G. Lehmann and K. H. Spatschek, Phys. Rev. Lett. **116**, 225002 (2016).
[4] P. Michel, L. Divol, D. Turnbull, and J. D. Moody, Phys. Rev. Lett. **113**, 205001 (2014); D. Turnbull *et al.*, Phys. Rev. Lett. **116**, 205001 (2016).
[5] S. Monchoce, S. Kahaly, A. Leblanc, L. Videau, P. Combis, F. Reau, D. Garzella, P. D'Oliveira, P. Martin, and F. Quere, Phys. Rev. Lett. **112**, 145008 (2014).
[6] V. M. Malkin, G. Shvets, and N. J. Fisch, Phys. Rev. Lett. **82**, 4448 (1999).
[7] V. M. Malkin, G. Shvets, and N. J. Fisch, Phys. Rev. Lett. **84**, 1208 (2000).
[8] B. Ersfeld and D. A. Jaroszynski, Phys. Rev. Lett. **95**, 165002 (2005).
[9] A. A. Andreev, C. Riconda, V. T. Tikhonchuk, and S. Weber, Phys. Plasmas **13**, 053110 (2006).
[10] J. Ren, W. Cheng, S. Li, and S. Suckewer, Nat. Phys. **3**, 732 (2007).
[11] N. A. Yampolsky, N. J. Fisch, V. M. Malkin, E. J. Valeo, R. Lindberg, J. Wurtele, J. Ren, S. Li, A. Morozov, and S. Suckewer, Phys. Plasmas **15**, 113104 (2008); **18**, 056711 (2011).
[12] V. M. Malkin and N. J. Fisch, Phys. Rev. E **80**, 046409 (2009).
[13] R. M. G. M. Trines, F. Fiuza, R. Bingham, R. A. Fonseca, L. O. Silva, R. A. Cairns, and P. A. Norreys, Phys. Rev. Lett. **107**, 105002 (2011).
[14] R. M. G. M. Trines, F. Fiúza, R. Bingham, R. A. Fonseca, L. O. Silva, R. A. Cairns, and P. A. Norreys, Nat. Phys. **7**, 87 (2011).
[15] G. Lehmann, F. Schluck, and K. H. Spatschek, Phys. Plasmas **19**, 093120 (2012).
[16] Z. Toroker, V. M. Malkin, A. A. Balakin, G. M. Fraiman, and N. J. Fisch, Phys. Plasmas **19**, 083110 (2012).
[17] S. Weber, C. Riconda, L. Lancia, J. R. Marques, G. A. Mourou, and J. Fuchs, Phys. Rev. Lett. **111**, 055004 (2013).
[18] C. Riconda, S. Weber, L. Lancia, J.-R. Marquès, G. A. Mourou, and J. Fuchs, Phys. Plasmas **20**, 083115 (2013).
[19] G. Lehmann, and K. H. Spatschek, Phys. Plasmas **20**, 073112 (2013).
[20] G. Lehmann, and K. H. Spatschek, Phys. Plasmas **21**, 053101 (2014).
[21] A. Frank *et al.*, Eur. Phys. J. Spec. Top. **223**, 1153 (2014).
[22] C. Riconda, S. Weber, L. Lancia, J.-R. Marquès, G. Mourou, and J. Fuchs, Plasma Phys. Controlled Fusion **57**, 014002 (2015).
[23] G. Lehmann, and K. H. Spatschek, Phys. Plasmas **22**, 043105 (2015).
[24] F. Schluck, G. Lehmann, and K. H. Spatschek, Phys. Plasmas **22**, 093104 (2015).
[25] M. Shoucri, J.-P. Matte, and F. Vidal, Phys. Plasmas **22**, 053101 (2015).
[26] X. Yang *et al.*, Sci. Rep. **5**, 13333 (2015).
[27] M. Chiaramello, C. Riconda, F. Amiranoff, J. Fuchs, M. Grech, L. Lancia, J.-R. Marquès, T. Vinci, and S. Weber, Phys. Plasmas **23**, 072103 (2016).
[28] M. R. Edwards, N. J. Fisch, and J. M. Mikhailova, Phys. Rev. Lett. **116**, 015004 (2016).
[29] G. Lehmann, and K. H. Spatschek, Phys. Plasmas **23**, 023107 (2016).
[30] F. Schluck, G. Lehmann, C. Müller, and K. H. Spatschek, Phys. Plasmas **23**, 083105 (2016).
[31] Q. Jia, I. Barth, M. R. Edwards, J. M. Mikhailova, and N. J. Fisch, Phys. Plasmas **23**, 053118 (2016).
[32] J. Fuchs *et al.*, Eur. Phys. J. Spec. Top. **223**, 1169 (2014).
[33] M. Nakatsutsumi, A. Kon, S. Buffechoux, P. Audebert, J. Fuchs, and R. Kodama, Opt. Lett. **35**, 2314 (2010).
[34] R. Wilson *et al.*, Phys. Plasmas **23**, 033106 (2016).
[35] International Zetawatt Exawatt Science Technology, http://www.izest.polytechnique.edu.
[36] G. A. Mourou, N. J. Fisch, V. M. Malkin, Z. Toroker, E. A. Khazanov, A. M. Sergeev, T. Tajima, and B. Le Garrec, Opt. Commun. **285**, 720 (2012).
[37] Extreme Light Infrastructure, https://www.eli-laser.eu.
[38] Exawatt Center for Extreme Light Studies, http://www.xcels.iapras.ru.
[39] D. W. Forslund, J. M. Kindel, and E. L. Lindman, Phys. Fluids **18**, 1002 (1975).
[40] B. Cohen and C. Max, Phys. Fluids **22**, 1115 (1979).
[41] I. N. Ross, in *Strong Field Laser Physics*, edited by T. Brabec (Springer, New York, 2008).
[42] L. Lancia *et al.*, Phys. Rev. Lett. **104**, 025001 (2010).
[43] L. Lancia *et al.*, Phys. Rev. Lett. **116**, 075001 (2016).
[44] P. Mounaix and D. Pesme, Phys. Plasmas **1**, 2579 (1994).
[45] P. Guzdar, C. S. Liu, and R. H. Lehmberg, Phys. Plasmas **3**, 3414 (1996).
[46] The growth rate γ_{SC} can be written in practical units as $(\gamma_{SC}/\omega_0) \approx 5.04\times10^{-8}(I_p[\mathrm{W/cm^2}]\lambda^2[\mu\mathrm{m}])^{1/3}[1-(n/n_c)]^{1/3}(n/n_c)^{1/3}(Z/A)^{1/3}$, where I_p, λ, and Z/A are the pump intensity, the wavelength in vacuum, and the ratio of charge and atomic number of the medium considered, respectively.
[47] D. Strickland and G. A. Mourou, Opt. Commun. **56**, 219 (1985).
[48] A. Dubietis, G. Jonušauskas, and A. Piskarskas, Opt. Commun. **88**, 437 (1992).
[49] A more complete analytical solution of the set of Eqs. (2) in different limits and where the spatial derivatives are taken into account will be published elsewhere.
[50] P. Michel *et al.*, Phys. Rev. Lett. **102**, 025004 (2009).